(will be inserted by hand later)

Dust formation in winds of long-period variables

V. The influence of micro-physical dust properties in carbon stars

A. C. Andersen[1,2], S. Höfner[1], and R. Gautschy-Loidl[3]

[1] Department of Astronomy & Space Physics, Uppsala University, P.O.Box 515, SE-751 20 Uppsala, Sweden
e-mail: hoefner@astro.uu.se
[2] Astronomical Obs., NBIfAFG, Copenhagen University, Juliane Maries Vej 30, DK-2100 Copenhagen, Denmark
e-mail: anja@astro.ku.dk
[3] Rüti, Switzerland
e-mail: rita@gautschy.com

Received ; accepted

Abstract. We present self-consistent dynamical models for dust-driven winds of carbon-rich AGB stars. The models are based on the coupled system of frequency-dependent radiation hydrodynamics and time-dependent dust formation. We investigate in detail how the wind properties of the models are influenced by the micro-physical properties of the dust grains that are required by the description of grain formation. The choice of dust parameters is significant for the derived outflow velocity, the degree of condensation and the resulting mass loss rates of the models. In the transition region between models with and without mass loss the choice of micro-physical parameters turns out to be very significant for whether a particular set of stellar parameters will give rise to a dust-driven mass loss or not.

Key words. hydrodynamics - radiative transfer - stars: mass loss - stars: atmospheres - stars: carbon - stars: AGB and post-AGB

1. Introduction

Mass loss by dust driven winds of asymptotic giant branch (AGB) stars is probably one of the major mechanism which recycle material in the Galaxy (e.g. Sedlmayr 1994). Most stars ($M_\star < 8M_\odot$) will eventually become AGB stars and subsequently end their life as white dwarfs surrounded by planetary nebulae.

AGB stars are cool ($T_\star < 3500$ K) and luminous ($L_\star$ of a few 10^3 to a few 10^4 $L_\odot$), and a majority of them are pulsating long-period variables (LPVs). The outer layers of many AGB stars provide favorable conditions for the formation of molecules and dust grains. Dust grains play an important role for the heavy mass loss (up to $\dot{M} \sim 10^{-4} M_\odot$/yr) of these stars by transferring momentum from the radiation to the gas.

Pulsation causes an extended atmosphere where the dust is condensing. The dust absorbs the light of the central star and re-radiates it at longer wavelengths in the infrared rage ($\lambda > 2\mu$m). The density of material in the circumstellar envelope may be so large that the star completely disappears in the visual rage. Considerable effort has been put into a theoretical description of the mass loss of AGB stars. At the end stages of stellar evolution the mass loss rates becomes so high that they (and not the nuclear burning rates) determine the stellar evolutionary faith. The goal is to develop a mass loss description that can be used as input to models of stellar evolution and the chemical evolution of the Galaxy.

This paper is the fifth in our series on dust formation in winds of long-period variables. The previous models presented in Paper I-IV are all based on gray radiative transfer while the models presented here are calculated using frequency dependent radiative transfer for the gas and dust (see Höfner et al. 2002 for details). Dynamic atmosphere models are undergoing a transition from qualitative modeling of physical processes to reliable quantitative predictions and interpretations of observations. For a given set of stellar parameters and elemental abundance, the mass loss rate, the outflow velocity and the degree of condensation is obtained by averaging the outflow of the time-dependent models.

In this paper we focus on the influence of the micro-physical (i.e. optical and chemical) properties of dust grains on the wind of AGB stars, to determine to what extent the choice of micro-physical parameters influences the overall mass loss predictions. As demonstrated in

Send offprint requests to: A.C. Andersen

Andersen et al. (1999) the choice of opacity was only of minor importance for the predicted mass loss rates in the gray models, however, for the frequency-dependent models the micro-physical properties of the dust grains affect the mean outflow velocity and the degree of condensation significantly.

In Sect. 2 we discuss the hydrodynamical models with emphasis on the treatment of the grain formation. Section 3 describes the different types of amorphous carbon dust used to test the model dependence on the choice of the micro-physical parameters. In Sect. 4 we present the results and show that the choice of opacity data, the values used for the sticking coefficients and the intrinsic dust density of the material, all affect the mass loss rate resulting from the models. This has an influence on the calculated synthetic colors which are compared with observations in Sect. 5. Conclusions are presented in Sect. 6.

2. The hydrodynamical model

Our spherically symmetric hydrodynamical models predict the mass loss rates of AGB stars by treating in detail the atmosphere and the circumstellar environment around pulsating long-period variable stars. This is done by solving the coupled system of radiation hydrodynamics and time-dependent dust formation (cf. Höfner et al. 2002) employing an implicit numerical method and an adaptive grid (for details on the numerical technique see Dorfi & Feuchtinger 1991).

2.1. Hydrodynamics and radiative transfer

In our models the radiation-hydrodynamical treatment of the stellar atmosphere apply a description with separate conservation laws for the dust, the gas and the radiation field. The resulting set of nonlinear partial differential equations for the gas and the radiation field consist of:
- equation of continuity (mass conservation)
- equation of motion (matter momentum conservation)
- equation of gas internal energy (energy conservation)
- 0. moment equation of the radiation (radiation energy conservation)
- 1. moment equation of the radiation (radiation momentum conservation)
- moment equations for the dust (grain formation and grain growth)
- Poisson equation (self gravitation).

For the dust component only certain moments of the grain size distribution have to be known for a complete description of the circumstellar envelope (more details in Sect. 2.2.1).

A system of 11 nonlinear partial differential equations plus the so-called grid equation which determines the locations of the grid points depending on some critical physical quantities to be resolved during the computations is solved.

The models presented here describe the radiation field by a frequency-dependent treatment of the gas and dust (Höfner 1999; Höfner et al. 2002) in contrast to earlier models in this series.

Basically four stellar parameters are needed as input; the stellar mass ($M_\star$), the effective temperature ($T_{\rm eff}$) and the luminosity ($L_\star$) of the star plus the gas abundance ratio ($\varepsilon_{\rm C}/\varepsilon_{\rm O}$) of carbon to oxygen. However, to describe the pulsation of the star, two additional parameters are required. Pulsation is simulated by a sinusoidal motion of the inner boundary R_{in} which is located below the stellar photosphere. This variable inner boundary is parameterized by a velocity amplitude (Δv) and a pulsation period (P). The luminosity at the inner boundary is variable and no mass flux is allowed across this boundary (Höfner & Dorfi 1997).

As in previous models a perfect gas law with $\gamma = 5/3$ and $\mu = 1.26$ is used as equation of state for reasons of comparison.

The models presented here are based on opacity sampling data of molecular opacities (SCAN data base, Jørgensen 1997) at 51 frequency points between 0.25 and 12.5 μm. Solving the frequency-dependent transfer increase the computation time per time step considerably. To keep the computation time at a reasonable level the spatial grid points available in the model are reduced from 500 to 100 compared to the gray models presented in e.g. Höfner & Dorfi (1997; Paper IV).

The dynamical calculations all start from a hydrostatic initial model. The radiative pressure on dust initiates an outward motion and the expansion is followed by the grid out to around 20–30 $R_\star$. At this radius the outer boundary is fixed, allowing for outflow. A model evolves for typically 100 years. The model calculation is stopped before a significant depletion of the mass inside the computational domain occurs.

2.2. Grain formation in the models

Dust influence the dynamics and thermodynamics of the stellar atmosphere by its opacity. To calculate this opacity we need to know the amount of dust present. Dust formation proceeds far from equilibrium and it is necessary to use a detailed time-dependent description to determine the degree of condensation and other relevant properties of the dust.

Dust is formed by a series of chemical reactions in which atoms or molecules from the gas phase combine to clusters of increasing size. The molecular composition of the gas phase determines which atoms and molecules are available for the cluster formation and grain growth. Dust formation begins with nucleation of critical clusters followed by growth to macroscopic dust grains.

2.2.1. Grain growth

In our models grain formation is treated by the so-called moment method (Gail & Sedlmayr 1988; Gauger et al. 1990). The moment method describes the time evolution

of an ensemble of dust grains of various sizes and requires the nucleation rate as external input. The equations include non-TE effects due to chemical and thermodynamical non-equilibrium.

In the moment method the size of a single dust grain is expressed in terms of the number of monomers (N) contained in the grain. A monomer represents the basic element the grain is built of, i.e. a certain species of atoms or molecules. The ensemble of the grains is described by the size distribution function $f(N,t)$ representing the number densities of dust particles in dependence of their size N. The number density $f(N,t)$ of dust grains containing N monomers is changed by four processes: creation of grains of size N by growth of smaller dust particles and by destruction of larger ones as well as destruction of grains with N monomers by growth or evaporation (see Gail & Sedlmayr 1988 and Gauger et al. 1990 for details).

As long as the size of the dust grains is small compared to the wavelength of the photons in the relevant frequency region of the radiation field, which is the case for late-type stars, the optical properties of the dust do not depend explicitly on the size spectrum $f(N,t)$ but only on a few moments (K_j) of the grain size distribution function defined by

$$K_j = \sum_{N=N_l}^{\infty} N^{j/d}\, f(N,t), \tag{1}$$

where d denotes the spatial dimension of the grains ($d = 3$ for spherical particles and 2 for planar structures) and N_l is the lower limit of the grain sizes which may be regarded as macroscopic in the thermodynamical sense. In the work presented here we use the value $d = 3$ (i.e. assume spherical grains) and $N_l = 1000$.

From the moments K_j it is possible to calculate quantities like the total number density of dust grains, the mean grain radius and the fraction of condensible material actually condensed into grains.

Considering grains large enough that their thermodynamical properties do not depend on the grain size and assuming that only molecules with up to a few monomers contribute significantly to the growth process the following set of moment equations can be derived (Gauger et al. 1990)

$$\frac{dK_0}{dt} = \mathcal{J} \tag{2}$$

$$\frac{dK_j}{dt} = \frac{j}{d}\,\frac{1}{\tau}\,K_{j-1} + N_l^{j/d}\,\mathcal{J} \qquad (1 \le j \le d). \tag{3}$$

Here Eq. 3 determines the grain production rate. The quantity $1/\tau$ is the net growth rate of the dust grains and $\mathcal{J}$ is the net transition rate per volume from cluster sizes $N < N_l$ to $N > N_l$, this can be interpreted as the local current density of clusters flowing up-wards in cluster size space at N from the region $N \ge N_l$ (Gail & Sedlmayr 1988).

The net growth rate $1/\tau$ contains the number densities of the chemical species which take part in the dust formation process. The relevant quantities are obtained by assuming chemical equilibrium in the gas phase at the gas temperature $T_{\rm g}$

$$\begin{aligned}\left(\frac{1}{\tau}\right)_{\rm CE} &= \sum_{i=1}^{I} i\,A_1\,v_{th}(i)\,\alpha(i)\,f(i,t) \\ &\qquad \left[1 - \frac{1}{\mathcal{S}^i}\frac{\mathcal{K}_i(T_{\rm d})}{\mathcal{K}_i(T_{\rm g})}\sqrt{\frac{T_{\rm g}}{T_{\rm d}}}\right] \\ &\quad + \sum_{i=1}^{I'} i\,A_1 \sum_{m=1}^{M_i} v_{th}(i,m)\,\alpha_m^c(i)\,n_{i,m} \\ &\qquad \left[1 - \frac{1}{\mathcal{S}^i}\frac{\mathcal{K}_{i,m}^r(T_{\rm g})}{\mathcal{K}_{i,m}^r(T_{\rm d})}\,\frac{\mathcal{K}_{i,m}^r(T_{\rm d})}{\mathcal{K}_{i,m}^r(T_{\rm g})}\right]\end{aligned} \tag{4}$$

where $\mathcal{K}$ denotes the dissociation constant of the molecule of the growth reaction and $\mathcal{K}^r$ is the dissociation constant of the molecule involved in the reverse reaction (see Gauger et al. 1990). $f(i)$ and $n_{i,m}$ are the number densities of the i-mers and the molecules containing i-mers which contribute to the grain growth, respectively. A_1 denotes the (hypothetical) monomer surface area, v_{th} the thermal velocities of the corresponding growth species and α the sticking coefficients. The supersaturation ratio $\mathcal{S}$ is defined by

$$\mathcal{S} = \frac{P_{\rm mon}}{P_{\rm sat}(T_{\rm d})}, \tag{5}$$

which is the ratio of the actual partial pressure of the monomers in the gas phase to the vapor saturation pressure with respect to the dust temperature $T_{\rm d}$. If the thermodynamical conditions allow the formation of dust grains the net transition rate $\mathcal{J}$ is assumed to be equal to the nucleation rate, i.e. the rate at which supercritical (stable) clusters are formed out of the gas phase.

The number densities of the molecules relevant to the dust formation are calculated assuming chemical equilibrium between H, H_2, C, C_2, C_2H and C_2H_2 after the fraction of carbon bound in CO has been subtracted. Nucleation, growth and destruction of dust grains are supposed to proceed by reactions involving C, C_2, C_2H and C_2H_2. The values of the elemental abundances are taken to be solar (Allen 1973) except for the carbon abundance which is considered as a free parameter. The dissociation constants $\mathcal{K}(T)$ have been extracted from the JANAF tables (Stull & Prophet 1971).

2.2.2. Grain nucleation

Nucleation is the first stage of the condensation process whereby a vapor transforms to a solid or liquid. This phase change requires some degree of supersaturation in order to drive the system through the relatively unstable reactive intermediates (clusters) between the atomic or molecular vapor and the macroscopic solid or liquid states. Presently no nucleation rates based on calculations of chemical pathways are available for the astrophysical

problem under consideration here. Consequently, the nucleation rate which is a function of temperature and supersaturation ($\mathcal{S}$) for a particular vapor is often calculated by either the classical homogeneous nucleation theory (Becker & Döring 1935; Feder et al. 1966) or by the related scaled homogeneous nucleation theory (Hale 1986).

The classical homogeneous nucleation theory was developed to describe the nucleation of volatile[1] materials such as water, hydrocarbons or alcohols at relatively low levels of supersaturation ($\mathcal{S} \sim 1.1 - 5.0$) and temperatures ($\sim 300$ K). The theory was as such not developed to deal with supersaturated refractory[2] vapors at high temperatures. The theory describes the formation of critical nuclei in a supersaturated vapor by means of thermodynamic quantities. The essential basic assumption of this approach is that the properties of the clusters in the nucleation regime are given by the extrapolation of the bulk properties even into the domain of very small clusters or the interpolation of thermodynamic properties between those of the molecules and the solid particles. With these assumptions both the thermodynamic functions such as entropy and enthalpy and the rate coefficients describing cluster formation and destruction become simple analytical functions of the cluster size N, which allow a straightforward calculation of the rate of formation of critical clusters.

A fundamental result of classical nucleation theory is the existence of a bottleneck for particle formation. The small unstable clusters which form at random from the gas phase have to grow beyond a certain critical size N_* which corresponds to a maximum in the free energy of formation and separates the domain of small unstable clusters from the large thermodynamically stable grains. The rate of grain formation is determined by the transition rate $\mathcal{J}_*$ between both regions. The existence of such a critical cluster size also holds in more realistic theories of cluster formation. However, a review of the available experimental literature by Nuth & Ferguson (1993) shows that no experimental data exists to support the application of classical nucleation theory to the condensation of refractory vapors. Refractory vapors seem to condense out at different supersaturation ratio than volatile materials.

The application of classical homogeneous nucleation theory in astrophysical discussions of grain formation is sharply criticized by Donn & Nuth (1985). There was some hope that scaled nucleation theory (Hale 1986) might be a better way to describe the condensation of refractory vapors, since this is a generalization of classical nucleation theory by scaling the relevant parameters to those of the vapor at the critical temperature and pressure. Although this form is a variation of the classical nucleation theory, agreement with experimental data for various molecular fluids is rather good (Martinez et al. 2001). As a result of this success scaled nucleation theory was subsequently applied to selected refractory nucleation data (Hale et al. 1989) with some success. However, comparison materials suggested that refractory materials, in general could not be described as accurately (i.e. significant deviations occur for lithium, magnesium and bismuth) as the molecular fluids to which the scaled nucleation theory was originally applied (Nuth & Ferguson 1993). It was shown by Martinez et al. (2001) that the reason for the poor agreement of scaled nucleation theory to certain refractory materials appear to be, at least in part, the result of using an overestimated value for the excess surface entropy for liquid metals. Martinez et al. (2001) conclude that refractory materials, as a class, seem to behave differently than the simple fluids studied in the original work by Hale (1986) and that the use of bulk liquid properties to describe a process involving small metallic clusters is problematic and that there therefore is a serious need for more and better nucleation data for refractory materials.

A better description of the nucleation of small refractory clusters, which are needed as input for the moment method, will most likely have to come from experiments since none of the present theories are good enough. However, for now we will use the classical nucleation theory for our model calculations. We are aware that in this way we introduce uncertainties to our dust description but with no significant improved theory we find it justified to use classical nucleation theory as a first crude approximation. Once an improved description is derived it will be relatively easy for us to change the description of nucleation in the code.

In the present models the supersaturation $\mathcal{S}$ is defined as the ratio of the partial pressure of carbon atoms in the gas phase divided by the saturated vapor pressure of solid carbon (Eq. 5). As shown in Gail & Sedlmayr (1988) $\mathcal{S}$ depends on the actual lattice temperature of the N-cluster.

The value $\mathcal{S} = 3$ is adopted after Gail & Sedlmayr (1987b) as the minimum value for grain nucleation to occur. As seen from Fig. 1, where the supersaturation ratio $\mathcal{S}$ and the corresponding nucleation rate $\mathcal{J}_*$ is shown for one of the calculated models, the value of $\mathcal{S}$ is on the order of 100 in the zone where nucleation occur.

3. Amorphous carbon dust

Amorphous carbon particles are considered to be the most common type of dust present in circumstellar envelopes of carbon-rich AGB stars. The infrared spectra of late-type stars generally show a dust emissivity law ($Q(\lambda) \sim \lambda^{-\beta}$) with a spectral index of $\beta \sim 1$ (e.g. Campbell et al. 1976; Sopka et al. 1985; Martin & Rogers 1987; Gürtler et al. 1995). A λ^{-1} behavior can be expected in a very disordered two-dimensional material like amorphous carbon (e.g. Huffmann 1988; Jäger et al. 1998). Graphite formation in AGB stars seem unlikely, because of the absence of the narrow band at 11.52 μm in the observed spectra and the overall shape of infrared graphite spectra which are proportional to λ^{-2} (e.g. Draine & Lee 1984). This is consistent with physical considerations, predicting the for-

[1] A material that readily evaporates.
[2] A material that vaporises only at high temperature.

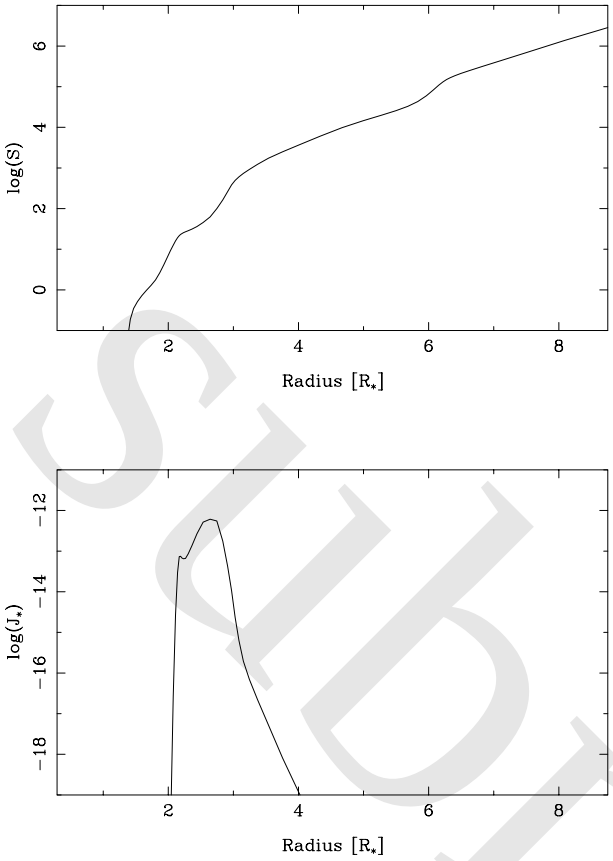

Fig. 1. A snapshot of the supersaturation $\mathcal{S}$ and the nucleation rate $\mathcal{J}_*$ for model l10dj10ρ199. The nucleation rate has a sharp maximum around $3R_\odot$ and at this point the supersaturation ratio is around 100.

mation of inhomogeneous grains with crystalline cores surrounded by amorphous mantles (Gail & Sedlmayr 1984).

3.1. Optical properties of dust

The formation of the dust grains influence the stellar atmosphere in two ways: In the gas phase chemistry, dust formation results in a depletion of certain elements, which influences the molecular composition of the gas, and consequently the corresponding opacities. On the other hand, dust grains have a rather high mass absorption coefficient which often may be comparable to the gas opacity or even exceed it. The total opacity of an ensemble of spherical dust grains can be formulated as

$$\kappa\left(\lambda\right) = \int_0^\infty a_{\rm gr}^2\, \pi\, Q_{\rm ext}\left(a_{\rm gr}, \lambda\right)\, n\left(a_{\rm gr}\right)\, da_{\rm gr}, \tag{6}$$

where $n\left(a_{\rm gr}\right) da_{\rm gr}$ is the number density of grains in the grain radius interval between $a_{\rm gr}$ and $a_{\rm gr} + da_{\rm gr}$ and $Q_{\rm ext}$ is the extinction efficiency, i.e. the ratio for the extinction cross section to the geometrical cross section of the grain (Bohren & Huffman 1983). This means that the size distribution function of the dust grains has to be known. However, if the particle size is small compared to the wavelength of the radiation the extinction efficiency ($Q_{\rm ext}$) is independent of the grain radius ($a_{\rm gr}$) and the dependence of the opacity on wavelength and grain size can be separated into two independent factors. The opacity of the dust particles in such a case only requires the knowledge of the moment K_3 since the extinction coefficient ($\kappa_{\rm ext}$) reduces to

$$\kappa_{\rm ext}(\lambda) = \frac{8\pi^2\, r_0^3}{\lambda}\, \Im\{\frac{m^2-1}{m^2+2}\} \cdot K_3, \tag{7}$$

here r_0 is the monomer radius

$$r_0 = \left(\frac{3 A_{\rm mon}\, m_p}{4\pi\, \rho_{\rm grain}}\right)^{1/3} \tag{8}$$

with $A_{\rm mon}$ being the atomic weight of the monomer (for carbon $A_{\rm mon} = 12.01115$), m_p the proton mass and $\rho_{\rm grain}$ is the intrinsic density of the condensed grain material. $\Im$ is the imaginary part and $m = n + ik$ is the complex index of refraction and

$$\kappa_{\rm sca}(\lambda) = \frac{128\pi^5\, r_0^6}{3\lambda^4}\, \Re\{\frac{m^2-1}{m^2+2}\}^2 \cdot K_6. \tag{9}$$

Thus in an astrophysical context, one is generally interested in the moments K_i for $i = 1, 2, 3$ if only the extinction coefficient is required and additionally in the moments with $i = 4, 5, 6$ if both absorption and scattering are required separately (Gail & Sedlmayr 1984).

The photospheric spectral energy distribution of AGB stars has its maximum around wavelengths of 1 μm (with a sharp decline of the stellar flux toward shorter wavelengths), and both observations and theoretical arguments indicate that typical grain sizes in these stars are smaller than 1 μm. Thus, the limit of particles being small compared to the wavelength is valid for a major fraction of the spectrum. We therefore do not need to specify details about the size distribution of the grains to calculate the grain opacities required for model atmospheres. However, it may still be necessary to know properties like the size distribution and shapes of the grains to compute detailed synthetic spectra at very short wavelengths. The needed complex refractive index of the material as a function of wavelength can be determined from laboratory measurements.

3.2. Laboratory measurements of amorphous carbon

Due to the nature of amorphous carbon dust materials they span a broad range of micro-physical properties. In the models presented here we have used three different laboratory measurements (*Jäger 1000, Jäger 400* and *Rouleau*, see Table 1) to describe the opacity of the dust grains formed in the circumstellar envelope.

The data by Jäger et al. (1998) are produced by pyrolizing cellulose materials at different temperatures. The materials are characterize in exemplary detail. In this study we have used the data synthesized at 400° C and 1000° C. The two materials differ in the bonding, where the *Jäger400* material has more single bonds (the carbon atoms are mainly sp^3 hybridized) while the *Jäger1000*

Table 1. List of the different dust opacities used.

Reference	Material name	$\rho_{\rm dust}$ (g/cm^3)	sp^2 %	Designation in this paper	Comments
Jäger et al. (1998)	cel400	1.435	67	*Jäger 400*	completely amorphous
Jäger et al. (1998)	cel1000	1.988	80	*Jäger 1000*	contains graphite (2 nm) crystallites
Rouleau & Martin (1991)	AC2	1.85	-	*Rouleau*	

material has more double bonds (the carbon atoms are mainly sp^2 hybridized). Reflectance spectra were obtained of the samples and from these the complex refractive index (m) was derived by the Lorentz oscillator method (see e.g. Bohren & Huffman 1983, Chap. 9).

Rouleau & Martin (1991) produced synthetic optical constants (n and k; $m = n + ik$) based on measurement of sub-micron amorphous carbon particles by Bussoletti et al. (1987). The particles were produced by striking an arc between two amorphous carbon electrodes in a controlled Ar atmosphere.

3.3. Grain equilibrium temperature

The presence of dust grains influences both the momentum and the energy balance of the atmosphere. We assume complete momentum coupling of gas and dust, which means that the momentum gained by the dust from the radiation field is directly transferred to the gas. On the other hand, the transfer of internal energy between gas and dust is negligible compared to the interaction of each component with the radiation field (cf. Gauger et al. 1990). We therefore assume that the grain temperature is given by the condition of radiative equilibrium

$$\chi_J\, J - \chi_S\, S_{\rm d} = 0 \;\;\Rightarrow\;\; T_{\rm d} = \left(\frac{\chi_J}{\chi_S}\right)^{\frac{1}{4}} T_{\rm r} \tag{10}$$

where the source function $S_{\rm d} = B(T_{\rm d})$, the frequency-integrated opacities are defined by

$$\chi_J \;=\; \frac{\int_\nu \chi_\nu\, J_\nu\, d\nu}{\int J_\nu\, d\nu} \tag{11}$$

$$\chi_S \;=\; \frac{\int_\nu \chi_\nu\, S_\nu\, d\nu}{\int S_\nu\, d\nu} = \frac{\int_\nu \chi_\nu\, B_\nu(T_{\rm d})\, d\nu}{\int B_\nu(T_{\rm d})\, d\nu} \tag{12}$$

and the radiation temperature $T_{\rm r} = (J\pi/\sigma)^{1/4}$.

For a gray opacity we would obtain $\chi_J \equiv \chi_S$ for the opacities and the temperatures $T_{\rm d} \equiv T_{\rm r}$ as in previous models. Using frequency-dependent radiative transfer the opacities χ_J and χ_S differ, for the data shown in Fig. 2, the absorption coefficient decrease with increasing wavelength in the infrared region of the spectrum, leading to $T_{\rm d} > T_{\rm r}$ for all data sets shown. The different between $T_{\rm d}$ and $T_{\rm r}$ becomes larger with an increasing slope of $Q_{\rm ext}(\lambda)/a($ and in the critical region around 1 μm where AGB stars have their photospheric flux maximum, the difference may reach several 10^2. In other words the steeper the dependence on wavelength, the larger the difference between the equilibrium grain temperature and the radiation temperature.

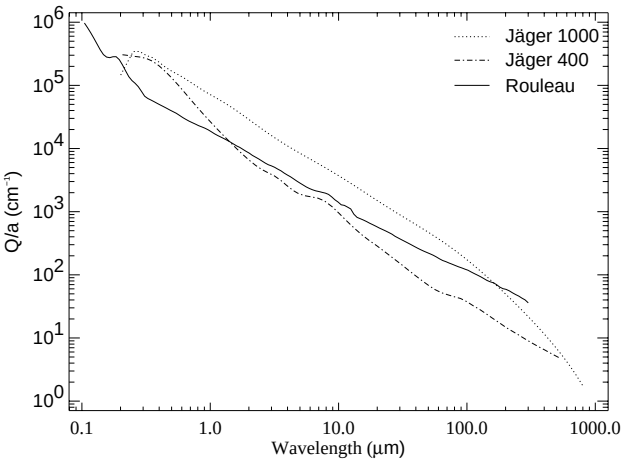

Fig. 2. Wavelength dependence of the dust absorption efficiency (see Table 1 for dust annotation).

The steeper slope of *Jäger 400* data result in a relatively high grain temperature compared to *Jäger 1000* and *Rouleau*.

4. Results

4.1. Wind properties

One of the main reasons for the huge mass loss of AGB stars seem to be the presence of newly formed dust grains. The strong shock waves in the stellar atmosphere, causes a levitation of the outer layers. The cool and relative dense environment which results from the levitation provides favorable conditions for the formation of molecules and grains. The dust formed have a strong influence on the structure and wind properties of the atmosphere.

4.1.1. Influence of the dust extinction

The influence of the dust extinction, on the structure and the wind of the dynamical models is shown in Table 2 and Fig. 3. The models are dependent on the choice of laboratory measurements of the opacity ($Q_{\rm ext}(\lambda)/a$) as already shown for gray models in Andersen et al. (1999). In contrast to the gray models, for the frequency-dependent models both the absolute value and the slope of the dust opacity data becomes relevant. The absolute value of the grain opacities mainly affect the terminal velocity of the

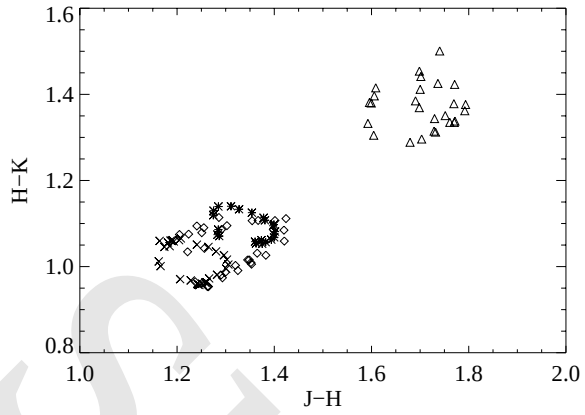

Fig. 3. The colors (J−H) vs. (H−K) of the four models l13dj10ρ199 ($\diamond$), l10dj10ρ199 ($\triangle$), l13drouρ185 ($\times$) and l10drouρ185 ($*$). There are two differences between the two sets of models. (1) The assumed value of the luminosity ($L_\star$) and corresponding effective temperature ($T_\star$), and (2) the dust opacity data used (*Jäger 1000* and *Rouleau*). All other model values are kept constant. See Table 2 for details.

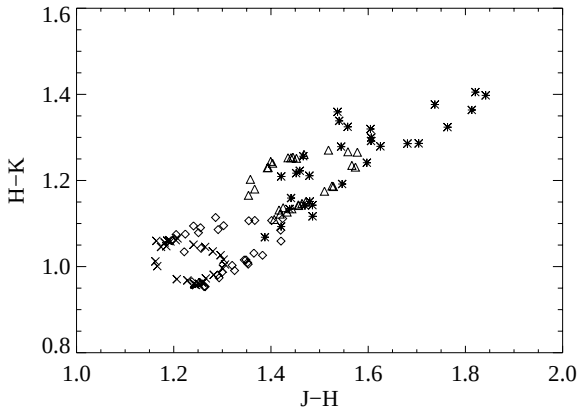

Fig. 4. The colors (J−H) vs. (H−K) for the four models l13dj10ρ199 ($\diamond$), l13dj10ρ225 ($*$), l13drouρ185 ($\times$) and l13drouρ225 ($\triangle$). We see the results for two different opacity data (*Jäger 1000* and *Rouleau*). Two different models for each opacity data are shown. The difference between the two models with the same opacity is the assumed value of the intrinsic density ($\rho_{\rm dust}$) of the dust material formed in the model. The values correspond to the one determined in the laboratory for the material and the value for graphite (2.25 g/cm^3) which was used in previous models. See Table 3 for details.

winds, while the slope of the grain opacity has significant influence on the grain temperature as discussed in Sect. 3.3. In the models where *Jäger 400* data is used for the opacity of the grains, the slope of the extinction efficiency as a function of λ dictates a high grain temperature which prevents dust formation. Models with identical stellar parameters based on *Jäger 1000* and *Rouleau* data on the other hand develop dust-driven winds.

Fig. 3 and Table 2 compared to the radiation temperature $T_{\rm r}$, show it is not possible to distinguish from near infrared photometry alone between the different models, since the hotter model using the *Jäger 1000* opacity data has similar color as the cooler model using the optical properties from the *Rouleau* data. However, the outflow velocity $\langle u \rangle$ (see Table 2) of the cooler *Rouleau* model is significantly less (by about a factor of 4) than for the hotter model using the *Jäger 1000* opacity data, indicating that it should be possible to distinguish by high-resolution spectroscopy.

4.1.2. Influence of the intrinsic dust density

When the moment method was developed by Gail & Sedlmayr (1988) the intrinsic density for the amorphous carbon used in that generation of models (Maron 1990) was not known. The value of graphite (2.25 g/cm^3) was therefore assumed. This value was later used in almost all existing models (e.g. Fleischer et al. 1992; Höfner & Dorfi 1997).

To test how much this assumption influences the results of the models we have calculated models with the optical properties represented by three different amorphous carbon materials for which the intrinsic density of the amorphous carbon material have been measured in the laboratory. These we compare with three models where the same opacity data were used but where we assumed the increased value for the intrinsic density of graphite instead of the measured value of the material, while keeping all other parameters constant.

The result of using the higher density of graphite instead of the correct value can be seen in Table 3 and Fig. 4. From Fig. 4 it is clear that the models become much redder when the intrinsic density of graphite is used instead of the value for amorphous carbon since significantly more dust is formed in these models. The huge increase in the mean degree of condensation $\langle f_{\rm c} \rangle$ at the outer boundary implies that more dust particles are formed, this results in an increased radiation pressure on the dust grains and the models therefore show an increase of the mean velocity ($\langle u \rangle$) at the outer boundary. Even a small increase of about 10% in the density of the dust material (as it is the case from model l13dj10ρ199 to l13dj10ρ225) results in a doubling of the degree of condensation and a substantial increase of the outflow velocity $\langle u \rangle$, and the mass loss rate. For the models l13drouρ185 and l13drouρ225 where the different value used for the intrinsic dust density is about 20%, the estimated mass loss rates differ almost by a factor of 2. For the models using the *Jäger 400* material (l13dj04ρ144 and l13dj04ρ225), where the difference is almost 40%, using the measured material value instead of the higher value for graphite results in a model that will not develop a wind at all.

The intrinsic dust density of the dust material is so significant for the obtained results because when the intrinsic dust density ρ_{grain} is increased the monomer radius r_0 decreases (see Eq. 8). This influences both the grain growth and the dust opacity. The net growth rate $1/\tau$ and the

Table 2. Influence of the extinction efficiency of the dust. *Model parameters:* $M_\star = 1.0\,M_\odot$, sticking coefficient $\alpha_C = 0.37$, $\alpha_{C_2} = 0.34$, $\alpha_{C_2H} = 0.34$ and $\alpha_{C_2H_2} = 0.34$, $\varepsilon_C/\varepsilon_O = 1.4$, period $P = 650$ d, piston velocity $\Delta u_p = 4$ km/s, luminosity $L_\star$, temperature $T_\star$, radius $R_\star$, dust opacity data κ_{dust}, intrinsic dust density ρ_{dust}; *Results:* Mass loss rate $\dot{M}$, mean velocity at the outer boundary $\langle u \rangle$, mean degree of condensation at the outer boundary $\langle f_c \rangle$.

Model	$L_\star$ [$L_\odot$]	$T_\star$ [K]	$R_\star$ [$R_\odot$]	κ_{dust}	ρ_{dust} [g/cm^3]	$\dot{M}$ [$M_\odot$/yr]	$\langle u \rangle$ [km/s]	$\langle f_c \rangle$	Symbol in Fig. 3
l13dj10ρ199	13000	2700	521	*Jäger 1000*	1.99	$5.59 \cdot 10^{-6}$	14.8	0.05	$\diamond$
l13drouρ185	13000	2700	521	*Rouleau*	1.85	$4.87 \cdot 10^{-6}$	7.38	0.10	$\times$
l13dj04ρ144	13000	2700	521	*Jäger 400*	1.44	-	-	-	-
l10dj10ρ199	10000	2600	493	*Jäger 1000*	1.99	$7.00 \cdot 10^{-6}$	16.3	0.10	$\triangle$
l10drouρ185	10000	2600	493	*Rouleau*	1.85	$2.26 \cdot 10^{-6}$	3.64	0.12	$*$
l10dj04ρ144	10000	2600	493	*Jäger 400*	1.44	-	-	-	-

Table 3. Influence of the intrinsic density of the dust. *Model parameters:* Same as Table 2.

Model	$L_\star$ [$L_\odot$]	$T_\star$ [K]	κ_{dust} g/cm^3	ρ_{dust} [$M_\odot$/yr]	$\dot{M}$ [km/s]	$\langle u \rangle$	$\langle f_c \rangle$	Symbol in Fig. 4
l13dj10ρ199	13000	2700	*Jäger 1000*	1.99	$5.59 \cdot 10^{-6}$	14.8	0.05	$\diamond$
l13dj10ρ225	13000	2700	*Jäger1000*	2.25	$7.26 \cdot 10^{-6}$	20.8	0.11	$*$
l13drouρ185	13000	2700	*Rouleau*	1.85	$4.87 \cdot 10^{-6}$	7.38	0.10	$\times$
l13drouρ225	13000	2700	*Rouleau*	2.25	$8.24 \cdot 10^{-6}$	18.1	0.31	$\triangle$
l13dj04ρ144	13000	2700	*Jäger400*	1.44	-	-	-	-
l13dj04ρ225	13000	2700	*Jäger400*	2.25	$2.10 \cdot 10^{-8}$	1.38	0.13	-

Table 4. Influence of the sticking coefficient for the dust formation. *Model parameters:* Same as Table 2 except for the sticking coefficients: α_C, α_{C_2}, α_{C_2H} and $\alpha_{C_2H_2}$, dust opacity κ_{dust} = *Rouleau*, and the intrinsic dust density $\rho_{dust} = 1.85$ g/cm^3 for all models.

Model	$L_\star$ [$L_\odot$]	$T_\star$ [K]	α_C	α_{C_2}	α_{C_2H}	$\alpha_{C_2H_2}$	$\dot{M}$ [$M_\odot$/yr]	$\langle u \rangle$ [km/s]	$\langle f_c \rangle$	Symbol in Fig. 5
l13drouρ185α03	13000	2700	0.37	0.34	0.34	0.34	$4.87 \cdot 10^{-6}$	7.38	0.10	$*$
l13drouρ185α02	13000	2700	0.20	0.20	0.20	0.20	$3.38 \cdot 10^{-6}$	3.87	0.09	-
l13drouρ185α05	13000	2700	0.50	0.50	0.50	0.50	$5.75 \cdot 10^{-6}$	10.5	0.12	-
l13drouρ185α10	13000	2700	1.00	1.00	1.00	1.00	$7.02 \cdot 10^{-6}$	16.5	0.22	$\triangle$
l10drouρ185α03	10000	2600	0.37	0.34	0.34	0.34	$2.26 \cdot 10^{-6}$	3.64	0.12	-
l10drouρ185α10	10000	2600	1.00	1.00	1.00	1.00	$6.95 \cdot 10^{-6}$	12.3	0.23	-

opacity κ dependent on the monomer radius as $1/\tau \sim r_0^2$ and $\kappa \sim r_0^3$. $1/\tau$ determines the amount of material that will condense in a particular model, while the opacity will determine the outflow velocity.

4.1.3. Influence of the estimated sticking coefficient

The sticking coefficient (also called the reaction efficiency factor) α enters into the net growth rate of the dust grains (Eq. 4). However, α is not definitely known as long as we do not know explicitly the sequence of chemical reactions responsible for the dust formation. To demonstrate how uncertainties in the value of α will influence the results of the models we have varied this parameter in otherwise identical models.

In the case of carbon dust formation the most important growth species is expected to be C_2H_2, but also C, C_2 and C_2H contribute to the growth (Gail & Sedlmayr 1988). In our earlier models we have used the values $\alpha_C = 0.37$, $\alpha_{C_2} = 0.34$, $\alpha_{C_2H} = 0.34$ and $\alpha_{C_2H_2} = 0.34$ to describe the grain growth.

Gail & Sedlmayr (1984) used the value $\alpha_C = 0.3$ adopted from Landolt-Börnstein (1968). Later Gail & Sedlmayr (1988) argued that the sticking coefficient α must be on the order of unity, because it is expected that neutral radical reactions play a dominant role in the formation process of carbon grains. However, if substantial energy barriers are involved in the reactions α may well be less by several orders of magnitude. It is important to remember that if α is small the assumption that nucleation can be treated as a time independent process will no longer hold. Small values of α should be accompanied by a time-dependent treatment of the dust nucleation (Gail & Sedlmayr 1988).

Salpeter (1973) has shown that the latent heat released when a monomer attaches itself to an N-mer may lead to a small sticking probability if N is small. Thus the sticking coefficient α for clusters with $N \approx N_*$ may be consider-

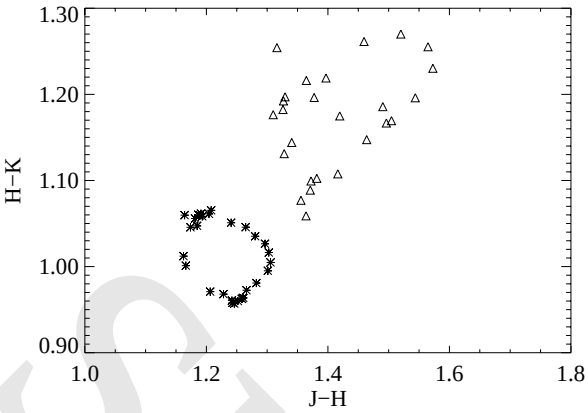

Fig. 5. The colors (J−H) vs. (H−K) for the two models l13drouρ185α03 ($*$) and l13drouρ185α10 ($\triangle$). The only difference between the two models is the assumed value of the sticking coefficient. The larger the sticking coefficient is assumed to be, the more efficient will the grain formation be and as a consequence the models will look redder when observed in (H−L), (J−H) or (K−L). See Table 4 for details.

ably smaller than the sticking coefficient for clusters with $N >> N_*$. The sticking coefficient is of the order unity for bulk material (Pound 1972).

To test the assumptions for the sticking coefficient we have calculated four models for a star with $L_\star$ = 13000 $L_\odot$, $T_\star$ = 2700 K and with the sticking coefficient (α) varying from $0.2 - 1.0$, two cooler models with $L_\star = 10000\ L_\odot$, $T_\star = 2600$ K and with the values $\alpha = 0.3$ suggested by Gail & Sedlmayr (1984) and the larger value $\alpha = 1$ suggested by Gail & Sedlmayr (1988).

It is clear from Table 4 and Fig. 5 (showing how the colors of two models depend on the chosen value for the sticking coefficient) that using the value of 1 as suggested by Gail & Sedlmayr (1988) compared to the values of 0.3 suggested by Gail & Sedlmayr (1984) results in a noticeable reddening of the colors of the stellar model. The reason for this reddening can be seen from Fig. 6, which shows the mean outflow velocity, the gas density, the gas temperature and the mean degree of condensation for four different phases of the two different models l13drouρ185α03 and l13drouρ185α10. The higher value of the sticking coefficient increases the degree of condensation and the outflow velocity by about a factor of 2, and therefore also the mass loss is increased.

From Fig. 6 it can be seen that dust formation occurs beyond $\approx 2R_\star$ independent of the value assumed for the sticking coefficient since the onset of condensation is determined mainly by the temperature. With the low choice of sticking coefficient ($\alpha = 0.3$) only about 10% of the condensable carbon material present in the gas actually condenses into grains, while for the much more favorable choice of sticking coefficient ($\alpha = 1$) twice as much material condenses into grains. A complete condensation of carbon grains is prevented by the rapid velocity increase after the onset of avalanche nucleation and the subsequent rapid dilution of the gas.

Table 5. Influence of the surface tension for the dust formation. *Model parameters:* Same as for model l13drouρ185 in Table 2 but with different values for the surface tension σ_{dust}.

Model	σ_{dust} [erg/cm^2]	$\dot{M}$ [M$_\odot$/yr]	$\langle u \rangle$ [km/s]	$\langle f_c \rangle$
l13drouρ185σ10	1000	$8.54 \cdot 10^{-6}$	35.2	0.76
l13drouρ185σ14	1400	$4.87 \cdot 10^{-6}$	7.38	0.10
l13drouρ185σ18	1800	-	-	-

4.1.4. Influence of the surface tension for the dust

In classical homogeneous nucleation theory, the surface function of the grain material is used to describe the gain of free entropy by forming a grain out of N monomers in the gas phase.

The surface tension $\sigma_{\rm dust}$ of amorphous carbon is not known from laboratory experiments, it has therefore become custom to use values for graphite, e.g. one of the values given by Tabak et al. (1975). One problem however is that there are huge variations in the values determined due to the anisotropy of graphite.

As already demonstrated by Tabak et al. (1975), varying the value of the surface tension may produce an enormous change in the nucleation rate. To determine how significant the prescribed value for the surface tension is for the results we have varied it around the value of 1400 erg/cm^2 which was used in previous models (see Table 5).

For the particular model, altering the value of the surface tension of the dust grains by 28% around the value of graphite will make the difference between obtaining a mass loss or not. The value of the surface tension also have a substantial influence on how much of the available material in the circumstellar envelope will condense into dust grains. For comparison, the measured surface tension for other materials are: Fe (σ_{dust} = 1400 erg/cm^2), MgS (σ_{dust} = 800 erg/cm^2) and SiO (σ_{dust} = 500 erg/cm^2) cf. Gail & Sedlmayr (1986).

5. Comparison with observations

Near-infrared colors including JHKL[3] magnitudes were calculated for a selection of the models. The filter zero points were calculated from a Vega model of Dreiling & Bell (1980), under the assumption that the Vega model has 0.0 mag in all filters.

Whitelock et al. (1997) presents observations of 11 large-amplitude carbon variables and Olivier et al. (2001) presents observations of 58 dust-enshrouded AGB stars from the solar neighborhood. From these samples we have

[3] Central filter wavelength [μm]: J = 1.22, H = 1.63, K = 2.19, L = 3.45.

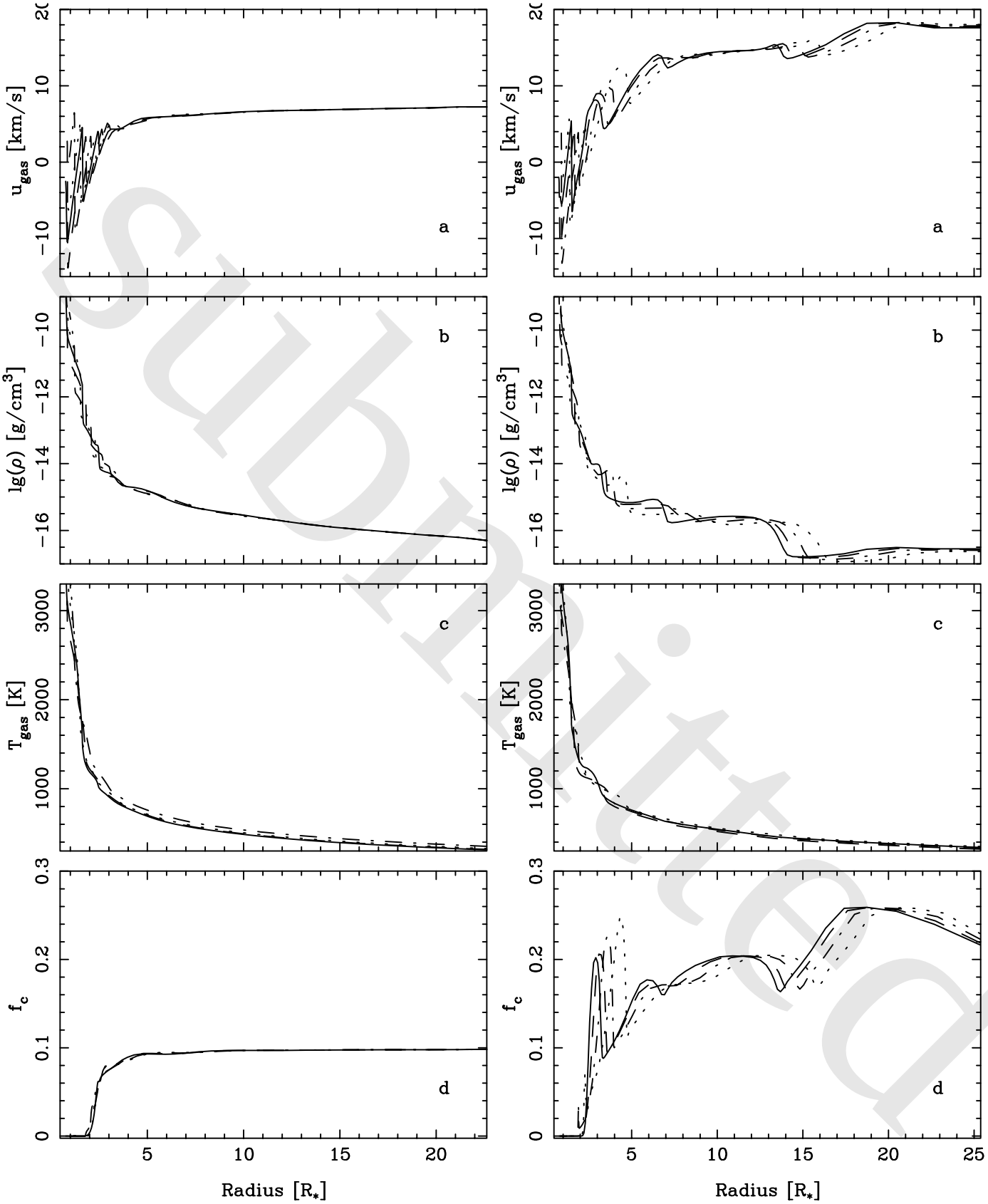

Fig. 6. Models l13drouρ185α03 (left) and l13drouρ185α10 (right). For four different phases of the two models (a) the mean outflow velocity of the gas, (b) the gas density, (c) the gas temperature and (d) the mean degree of condensation is shown. The only difference between the two models is the value used for the sticking coefficient. It is evident that the choice of sticking coefficient has a significant influence on the predicted outflow velocity $\langle u \rangle$ and the degree of condensation $\langle f_c \rangle$.

Table 6. Data from Whitelock et al. (1997) and Olivier et al. (2001) for carbon-rich Mira's with mass loss comparable to the models presented in the Tables 2, 3 and 4. The JHKL data are near-infrared magnitudes.

Star	Period [days]	J	H	K	L	$v_{\rm out}$ [km/s]	$\dot{M}$ [$M_\odot$/yr]	Symbol in Fig. 7
IRAS 10131+3049 (RW LMi)	640	6.12	3.42	1.27	-1.34	16.9	$7.59 \cdot 10^{-6}$	○
IRAS 10491-2059 (V Hya)	530	2.97	1.18	-0.09	-1.66	14.2	$1.82 \cdot 10^{-6}$	△
R Vol	454	4.68	2.87	1.56	0.04	20.0	$1.78 \cdot 10^{-6}$	∗
R For	389	3.70	2.12	0.96	-0.22	20.0	$1.23 \cdot 10^{-6}$	×
R Lep	427	2.10	0.79	-0.11	-0.99	20.0	$7.94 \cdot 10^{-7}$	
RV Cen	446	3.07	1.89	1.38	0.88	15.0	$2.51 \cdot 10^{-7}$	◇

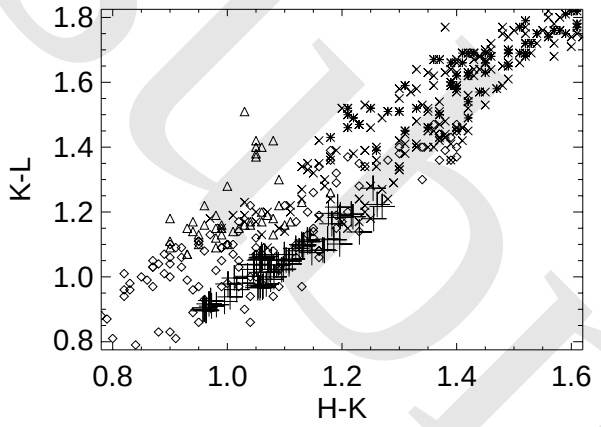

Fig. 7. The colors $(H-K)$ and $(K-L)$ for the models (+) l13drouρ185, l13drouρ185α10, l10drouρ185, and carbon Mira's with comparable mass loss rates (see Table 6); V Hya (△), R Vol (∗), R For (×), RV Cen (◇), R Lep (), RW LMi (○).

picked the carbon-rich stars with mass loss rates (Table 6) comparable to our models.

The mass loss rates were estimated by Whitelock et al. (1997) and Olivier et al. (2001) by the mass loss expression from Jura (1987):

$$\dot{M} = 1.7 \times 10^{-7}\, v_{15}\, r_{kps}^2\, L_4^{-\frac{1}{2}}\, F_{\nu,60}\, \bar{\lambda}_{10} \qquad (13)$$

where v_{15} is the outflow velocity of the gas in units of 15 km/s, $r_{\rm kpc}$ the distance to the star in kpc, L_4 the luminosity in units of $10^4 L_\odot$, $F_{\nu,60}$ the flux measured at 60 μm in Jansky and $\bar{\lambda}_{10}$ the mean wavelength of light emerging from the star and its circumstellar dust-shell in units of 10μm. The expression assumes all the grains to have an emissivity of 150 cm^{2}g^{-1} at 60μm and a dust to gas ratio of 4.5×10^{-3}. The outflow velocities, v_{15}, were taken to be the expansion velocity of the shell obtained from CO$(1 \rightarrow 0)$ line measurements.

The assumed grain emissivity of 150 cm^{2}g^{-1} at 60μm in Eq. 13 seems a bit high since the laboratory amorphous carbon material that we have used here (see Table 1) have values of 141 cm^{2}g^{-1}, 29 cm^{2}g^{-1} and 74 cm^{2}g^{-1} at 60μm for *Jäger 1000*, *Jäger 400* and *Rouleau* respectively.

A dust to gas ratio of 4.5×10^{-3} in Eq. 13 is also high compared to the models. The dust-to-gas mass ratio $\rho_{\rm d}/\rho_{\rm g}$ is related to the degree of condensation $f_{\rm c}$ by

$$\frac{\rho_d}{\rho_g} = \frac{m_{\rm C}}{m_{\rm H} + m_{\rm He}\,\varepsilon_{\rm He}}\,(\varepsilon_{\rm C} - \varepsilon_{\rm O})\; f_{\rm c} \qquad (14)$$
$$= \frac{12}{1.4}\,(\varepsilon_{\rm C}/\varepsilon_{\rm O} - 1)\,\varepsilon_{\rm O}\, f_{\rm c}$$

where $m_{\rm C}$, $m_{\rm H}$ and $m_{\rm He}$ are the atomic masses of carbon, hydrogen and helium, and $\varepsilon_{\rm C}$, $\varepsilon_{\rm O}$ and $\varepsilon_{\rm He}$ are the element abundance of C, O and He. ($\varepsilon_{\rm He} = 0.1$, $m_{\rm C}/m_{\rm H} = 12$, $m_{\rm He}/m_{\rm H} = 4$; $\log(\varepsilon_{\rm O}) = -3.18$). For models l13drou$\rho$185, l10drou$\rho$185, l10dj10$\rho$199 the dust to gas ratio ($\rho_{\rm d}/\rho_{\rm gas}$) is on the order of 2×10^{-4} and for the models l13drouρ185α10 and l10drouρ185α10 we have $\rho_{\rm d}/\rho_{\rm gas}$ around 5×10^{-4}. Using Eq. 13 will therefore give a higher optical depth than we find with our self-consistent models.

6. Conclusions

We have investigated in detail how the predicted wind properties of carbon-rich AGB models are influenced by the choice of micro-physical dust parameters (i.e. the optical properties of the dust, the intrinsic dust density, the assumed sticking coefficients and the surface tension of the grain material - these two last parameters control the efficiency of the dust formation).

For the theoretical predictions of mass loss it is important to know how the uncertainty in the chosen dust parameters affects the obtained results. Varying the micro-physical parameters within the rage typical of possible materials can change the value for the mean outflow velocity of the gas and dust by a factor of 4, the predicted degree of dust condensation by a factor of 10 and the predicted mass loss by a factor of 2. In the transition region between models with and without mass-loss the choice of micro-physical parameters is vital for whether a particular set of stellar parameters will give rise to a dust-driven mass loss or not.

The main source of momentum for the stellar wind is the radiation pressure on dust. The radiation pressure on the dust and the radiative equilibrium grain temperature is determined by the wavelength dependence of the grain extinction efficiency. The steeper the dependence of wavelength, the larger the difference between the equilibrium grain temperature and the radiation temperature. The radiation pressure on the other hand is proportional to the

flux mean opacity which both depends on the slope of the extinction efficiency as a function of wavelength and on its absolute value. The latter may differ by almost an order of magnitude for different types of amorphous carbon in the critical region around 1 μm. The density of the grain material has to be chosen consistently with the grain extinction efficiency.

The surface tension and the sticking coefficient is very significant for the calculated rates at which grains are formed out of the gas (nucleation) and at which new material is added to existing grains (grain growth). Even a moderate variation of the values within the range expected for possible materials has noticeable consequences for the properties of the dust-driven stellar winds, including the resulting near-infrared colors.

Acknowledgements. ACA gratefully acknowledges support from the Carlsberg Foundation. This work was supported by NorFA, the Swedish Research Council (VR) and the Royal Swedish Academy of Sciences (KVA).

References

Allen C.W., 1973, Astrophysical Quantities, The Athlone Press, London
Andersen A., Loidl R., Höfner S., 1999, A&A 349, 243
Becker R., Döring W., Ann. Physik, A125, 719
Bohren C.F., Huffman D.R., 1983, Absorption and Scattering of Light by Small Particles (John Wiley & Sons, New York)
Bussoletti E., Colangeli L., Borghesi A., Orofino V., 1987, A&AS 70, 257
Campbell M.F., Harvey P.M., Hoffmann W.F., Elias J.H., Neugebauer G., Gezari D.Y., Westbrook W.E., Hudson H.S., Soifer B.T., Werner M.W., 1976, ApJ 208, 396
Donn B., Nuth J.A.III., 1985, ApJ 288 187
Dorfi E., Feuchtinger M., 1991, A&A 29, 417
Draine B.T., Lee H.M., 1984, ApJ 285, 89
Dreiling L.A., Bell R.A., 1980, ApJ 241, 736
Feder J., Russel K.C., Lothe J., Pound G.M., 1966, Advances in Physics 15, 111
Fleischer A.J., Gauger A., Sedlmayr E., 1992, A&A 266, 321
Gail H.-P., Sedlmayr E., 1984, A&A 132, 163
Gail H.-P., Sedlmayr E., 1986, A&A 166, 225
Gail H.-P., Sedlmayr E., 1987a, A&A 171, 197
Gail H.-P., Sedlmayr E., 1987b, A&A 177, 186
Gail H.-P., Sedlmayr E., 1988, A&A 206, 153
Gauger A., Gail H.-P., Sedlmayr E., 1990, A&A 235, 345
Gürtler J., Kömpe C., Henning Th., 1996, A&A 305, 878
Hale B.N., 1986, Phys. Rev. A 33, 4156
Hale B.N., Kemper P., Nuth J.A.III., 1989, J. Chem. Phys. 91, 4314
Höfner S., 1999b, A&A 346, L9
Höfner S., Dorfi E.A., 1997, A&A 319, 648
Höfner S., Gautschy-Loidl R., Aringer B., Jørgensen U.G., 2002, submitted to A&A
Huffmann D.R., 1988, in Experiments on Cosmic Dust Analogues, Kluwer Academic Publishers, eds. E. Bussoletti, C. Fusco, G. Longo, 25
Jäger C., Mutschke H., Henning Th., 1998, A&A 332, 291
Jura M., 1987, ApJ 313, 743
Jørgensen U.G., 1997, In: van Dishoeck E.F. (ed.) Mulecules in Astrophysics: Probes and processes, [Kluwer], IAU Symp. 178, 441
Landolt-Börnstein, 1968, Zahlenwerte und Funktionen, vol. 5b, Springer Verlag, Berlin
Martin P.G., Rogers C., 1987, ApJ 322, 374
Martinez D.M., Ferguson F.T., Heist R.H., Nuth J.A.III., 2001, J. Chem. Phys. 115, 310
Maron N., 1990, Ap&SS 172, 21
Nuth J.A., Ferguson F., 1993, Ceramic Transactions 30, 23
Olivier E.A., Whitelock P., Marang F., 2001, MNRAS 326, 490
Pound G.M., 1972, J. Phys. Chem. Ref. Data 1, 135
Rouleau F., Martin P.G., 1991, ApJ 377, 526
Salpeter E.E., 1973, J. Chem. Phys. 58, 4331
Sedlmayr E., 1994, in Molecules in the Stellar Environment, LNP 428, ed. U.G. Jørgensen (Springer, Berlin), 163
Sopka R.J., Hildebrand R.H., Jaffe D.T., et al., 1985, ApJ 294, 242
Stull D.R., Prophet H., 1971, JANAF Thermochemical Tables, 2nd Ed., Nat. Bureau of Standards, Washington, (NSRDS-NBS37)
Tabak R.G., Hirth J.P., Meyrick G., Roark T.P., 1975, ApJ 196, 457
Whitelock P., Feast M., Marang F., Overbeek M., 1997, MNRAS 288, 512